Quantum vibrational resonance in a dual-frequency driven Tietz-Hua quantum well

O. I. Olusola,[1] O. P. Shomotun,[1] U. E. Vincent,[2, 3, *] and P. V. E. McClintock[2]

[1]*Department of Physics, University of Lagos, Lagos, Nigeria*
[2]*Department of Physics, Lancaster University, Lancaster LA1 4YB, United Kingdom*
[3]*Department of Physical Sciences, Redeemer's University, Ede, Nigeria*
(Dated: May 12, 2020)

We investigate the response of a quantum particle in the Tietz-Hua quantum potential driven by biharmonc fields – a low and a very high-frequency force. The response is characterized by the occurrence of a maximum in the first-order transition probability amplitude, $|s|^2$, under the influence of the applied fields. It is shown that in the absence of the high-frequency component of the applied fields, $|s|^2$ shows a distinct sequence of resonances; whereas an increase in the amplitude of the high-frequency field induces minima in $|s|^2$. However, the $|s|^2$ maximum occurs in the low-frequency regime where it may be considered otherwise weak in the presence of a single harmonic force.

I. INTRODUCTION

Periodically driven systems have attracted much attention over the years. They are ubiquitous in many different scientific and engineering disciplines. Driving functions can either be due to deterministic forces (i.e. single or multiple harmonic function of time) [1] or stochastic forces (i.e. forces in the form of noise) [2]. Periodic driving can induce a plethora of dynamical phenomenon that yield helpful insights into a wide range of processes on both the macroscopic and microscopic scales. They can give rise to more complex dynamics [3], to the suppression of synchronization when acting as coupling function [4] or to enhanced synchronization in the case of noise driving [5], to dissociation dynamics [6], and to nonlinear resonances [3, 7, 8], to mention but a few examples.

Vibrational resonance (VR), a nonlinear resonance phenomenon with potential applications to weak signal enhancement and bearing fault detection, has recently received considerable attention. The phenomenon occurs in bi-harmonically driven nonlinear systems. It was first identified and demonstrated numerically by Landa and McClintock [9], confirmed theoretically by Gitterman [10] and by Blekhman and Landa [11, 12] and detected experimentally in vertical cavity surface emitting lasers and optical systems [13–17]. In VR, the response of a nonlinear system to the effect of the low-frequency (LF) component of the bi-harmonic signal can be amplified by the presence of the high-frequency (HF) component when the difference between the frequencies is sufficiently large ([7, 15, 18–28] and references therein). The VR scenario is analogous to *stochastic resonance* (SR) but with the high-frequency input force taking the place of noise [29, 30]. Both SR and VR have been extensively investigated in the classical domain, and increasing effort is now being directed towards the study of quantum SR in a variety of systems [31–36]. Quantum VR has been much less studied [7, 18], however, and this is especially the case for systems with interatomic potentials describing the molecular dynamics at moderate and high rotation vibration quantum numbers [37].

Interatomic potentials arise in e.g. molecular physics, molecular mechanics and material science, in various forms – the most commonly used being the Morse [38] and Tietz-Hua [39] potentials that have largely replaced the more traditional Lennard-Jones potential. The Tietz-Hua (TH) potential is a much more realistic model than the Morse potential. It is known to provide an adequate description of the vibrational and rotational energy spectra, dissociation energies, and inter-molecular interactions of diatomic molecules. It was introduced by Wei Hua [39] as a four-parameter potential function for bond-stretching vibrations of diatomic molecules, and for fitting the experimental Rydberg-Klein-Rees (RKR) curve function. Extensive research has been carried out to obtain the eigenstates, intersubband optical transitions and energy eigenvalues, among others, of the potential for diatomic molecules, with applications in diverse optical and electronic systems [37, 40–46].

More importantly, the Tietz-Hua quantum well has been studied under two-frequency applied external fields. These included an intense laser field (ILF) plus lower frequency electric and magnetic fields. In this direction, the density matrix formalism and the perturbation expansion method were recently employed to investigate the optical transitions between any two subbands in the Tietz-Hua quantum well [47]. In related theoretical work, Ungan et al. [48] showed that changes in the Tietz-Hua potential quantum well refractive index and optical absorption coefficient are sensitive to the effects of applied external fields. The results [47, 48] demonstrate clearly that the intensity of the ILF and the strengths of the electric and magnetic fields may play significant roles in determining

* Corresponding author: u.vincent@lancaster.ac.uk

the nonlinear optical response of the Tietz-Hua quantum system. Motivated by these earlier results, we now explore VR in a TH quantum well. We characterize the response of the oscillator on the basis of the first-order transition probability and examine VR for the cases of positive, negative and zero potential constant. The rest of the paper is organized as follows. In Sec. II, we describe the Tietz-Hua quantum well. In Sec. III, we discuss our numerical results. Section IV discusses the parameter space of QVR including, in particular, the transition between resonance and antiresonance. The paper is summarized and concluded in Sec. V.

II. MODEL

When driven by a dual-frequency external field, namely, $W(t) = g\cos(\omega t) + G\cos(\Omega t)$ with $\Omega \gg \omega$, ω and Ω being the frequencies of the low and very high-frequency forces and g and G denoting their amplitudes, respectively; the Hamiltonian of the Tietz-Hua quantum mechanical oscillator under consideration is given by

$$H = H_0 + \lambda x(g\cos(\omega t) + G\cos(\Omega t)), \qquad (1)$$

where $H_0 = \frac{p_x^2}{2m} + V_{TH}$ is the unperturbed Hamiltonian of the system and V_{TH} is the confinement potential. In this study, V_{TH} is the Tietz-Hua (TH) potential given by [39],

$$V_{TH} = V_0 \left[\frac{1 - e^{-b_h(r-r_e)}}{1 - c_h e^{-b_h(r-r_e)}} \right]^2, b_h = \beta(1 - c_h) \quad (2)$$

where β stands for the Morse constant, V_0 is the depth of the potential, c_h is the potential constant representing an optimization parameter derived from an *ab-initio* or Rydberg-Klein-Rees (RKR) intra-molecular potential, r_e is the molecular bond length and b_h represents the confinement parameter, respectively. The potential is non-polynomial and, for positive values of V_0, V_{TH} has a minimum value of zero at $r = r_e$. In the interval $\Re^+ : c_h \in]-1, 1[$, V_{TH} is not a continous function, but has a singularity. In this paper, and for ease of calculation, we define a dimensionless parameter $x = \frac{r}{r_e}$, so that the TH potential takes the form

$$V_{TH}(x) = V_0 \left[\frac{1 - e^{-\gamma(x-1)}}{1 - c_h e^{-\gamma(x-1)}} \right]^2, \qquad (3)$$

where $\gamma = b_h r_e$. Remarkably, the TH potential reduces to the classical Morse potential [38] when the potential constant, $c_h = 0$, and becomes wider (narrower) for small (large) values of γ i.e.,

$$V_M(x) = V_0[1 - e^{-\gamma(x-1)}]^2. \qquad (4)$$

The essential features of the TH-potential are shown in Fig. 1 for the parameters $\gamma = 1$, $V_0 = 6$, and three values of c_h.
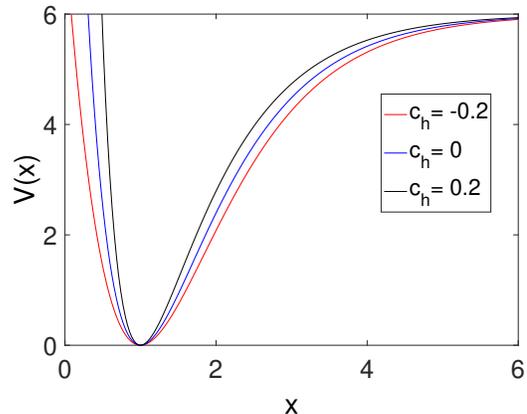

FIG. 1. (Colour online) The shape of the Tietz-Hua potential for the parameters $\gamma = 1$, $V_0 = 6$ and different values of c_h.

Our interest lies in calculating the probability of finding the oscillator in any f_{th} state at time t as the oscillator undergoes transitions between energy eigenstates when subjected to the external field. This probability is given by $P_{f_i}(T) = |\delta_{f_i} + \lambda a_f^{(1)}(T)|^2$ and its detailed derivation is presented in the *Appendix*. The term s in the expression for $a_f^{(1)}(T)$ depends solely on the parameters g, ω, G and Ω of the bi-harmonic forcing and T. Thus, the quantity of interest is $|s|^2$ and its variation with the parameters of the bi-harmonic force. The unperturbed Hamiltonian for the Tietz-Hua oscillator is exactly solvable for the s-wave $(l = 0)$ [42]. The energy eigenvalues were obtained and given in closed form as [42],

$$(2n+1)\left[\sqrt{A + BC^2} + c_h\sqrt{(V_0 - E_{n,0})\frac{B}{D}} \right] + BC$$

$$+ 2\sqrt{[A + BC^2]\left[\left(\frac{B}{V_0}\right)(V_0 - E_{n,0})\right]} + c_h^* = 0 \quad (5)$$

where $c_h^* = c_h(n^2 + 3n + 0.5) = 0$, $A = \frac{c_h}{4}$, $B = 2\mu\left(\frac{V_0}{b_h^2\hbar^2}\right)$, $C = (c_h - 1)$.

The Tietz-Hua quantum oscillator has a finite number of bound states for diatomic molecules, all of which can be controlled by the effective well depth parameter, V_0. For the purpose of our study we fix $V_0 = 100$ and set the quantities $\hbar^2 = 2\mu = b_h^2 = 1$ for convenience. The values of c_h are chosen to be [-0.2,0,0.2]. The closed form equation for the energy eigenvalue is then numerically evaluated at the set values to yield five bound states ($n = 0$, 1, 2, 3 and 4) for the different cases of the potential constant. All state transitions are referenced with respect to the ground state. Table I gives the corresponding energy levels and transition frequencies for the three values of the potential constant used in this paper.

TABLE I. Energy values and transition frequencies for Tietz Hua potential

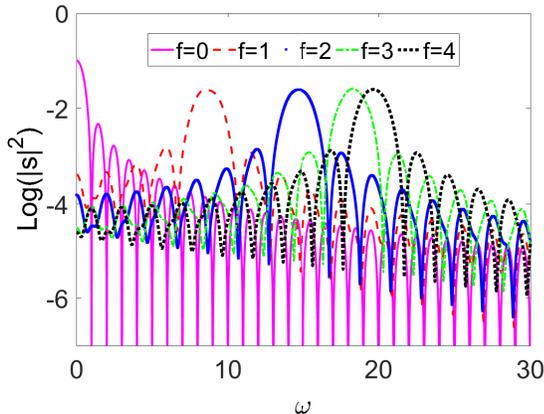|	$c_h = -0.2$		$c_h = 0$		$c_h = 0.2$	
n	$E_{n,0}$	ω_{f_i}	$E_{n,0}$	ω_{f_i}	$E_{n,0}$	ω_{f_i}
0	-20.6283	0	-20.25	0	-19.6949	0
1	-13.1625	7.465766	-12.25	8	-11.0152	8.679681
2	-7.28898	13.33933	-6.25	14	-4.96873	14.72615
3	-3.08509	17.54322	-2.25	18	-1.36033	18.33454
4	-0.63537	19.99295	-0.25	20	-0.01661	19.67826

FIG. 2. (Color Online) Resonance peaks in the low-frequency force regime of Tietz-Hua quantum oscillator with positive potential constant, $c_h = 0.2$: (a) $f = 0$; (b) $f = 1$; (c) $f = 2$; (d) $f = 3$; (e) $f = 4$.

III. RESULTS AND DISCUSSIONS

A. FIRST-ORDER PROBABILITY AMPLITUDE FOR LOW-FREQUENCY FORCE

Here, we examine the system in the absence of high-frequency force. Thus, we present numerical results for the first-order probability amplitude $|s|^2$ under the action of low-frequency excitation by assuming a finite time of application of external harmonic force, i.e. $T = 2\frac{\pi}{\omega}$ and that the system is initially in the ground state ($i = 0$). The amplitude of the low-frequency force is fixed as $g = 0.05$ throughout the paper. The low-frequency ω is varied from 0 to 30 to capture essential features of the resonances with their corresponding peaks. Results obtained for three cases, namely, positive, negative and zero potential constant are presented in Figures 2–4. The maximum transition probability amplitude for each of the three cases considered occurs when the frequency of the low-frequency driving force is equal to the transition frequency of that state. This follows directly from Eq. (18): when $\omega_{fi} \approx \omega$ the denominator in $r_{1-} \to 0$. Thus, the quantity r_{1+} can be neglected and the quantity $|s|^2$ attains its maximum value.

With positive potential constant, $c_h = 0.2$, we show in Fig. 2 a sequence of resonance peaks obtained for the
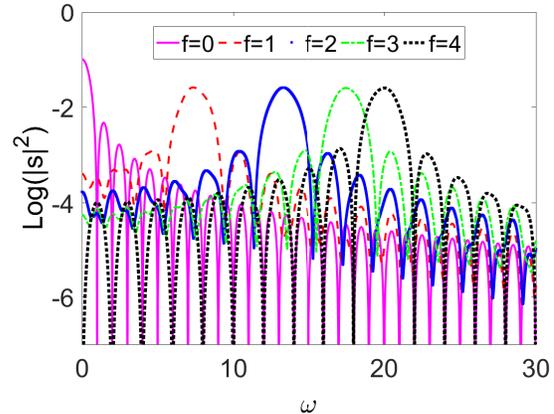

FIG. 3. (Color Online) Resonance peaks in the low-frequency force regime of Tietz-Hua quantum oscillator with negative potential constant, $c_h = -0.2$: (a) $f = 0$; (b) $f = 1$; (c) $f = 2$; (d) $f = 3$; (e) $f = 4$.
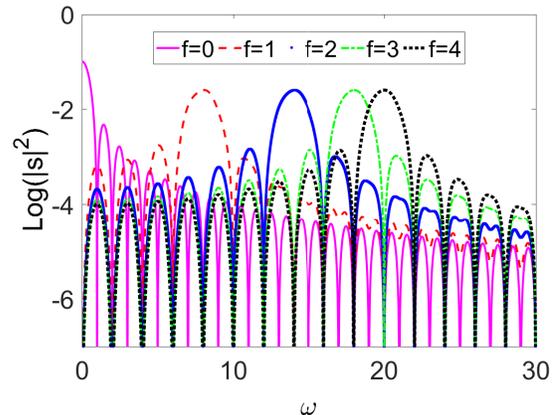

FIG. 4. (Color Online) Resonance peaks in the low-frequency force regime of Tietz-Hua quantum oscillator with zero potential constant, $c_h = 0$: (a) $f = 0$; (b) $f = 1$; (c) $f = 2$; (d) $f = 3$; (e) $f = 4$.

stationary states $f = 0, 1, 2, 3$ and 4, respectively. The transition frequencies are given in Table I. At $\omega = 0$, the quantity $|s|^2$ is maximum for state $f = 0$, while for the states $f = 1, 2, 3$ and 4 the quantity $|s|^2$ has the values 0.000407, 0.000152, 2.99 $\times 10^{-5}$ and 2.42×10^{-5}, respectively. The maximum peaks are obtained for each state at $\omega_{f_i} = \omega$ as can be seen from Fig. 2.

Shown in Fig. 3 is a sequence of resonance peaks obtained for the states $f = 0, 1, 2, 3$ and 4, respectively, using a negative potential constant, $c_h = -0.2$. The transition frequencies are given in Table I. Similar to the results for $c_h = 0.2$, at $\omega = 0$, the quantity $|s|^2$ is maximum for state $f = 0$, while for the states $f = 1, 2, 3$ and 4 the quantity $|s|^2$ has the values 0.000397,0.000167, 5.62×10^{-5} and 1.23×10^{-8}. Furthermore, the sequence of resonance peaks obtained for the states $f = 0, 1, 2, 3$ and 4, respectively are depicted in Fig. 4 for $c_h = 0$. The

transition frequencies are tabulated in Table I. $|s|^2$ takes on its maximum value at $\omega = 0$ for state $f = 0$ while for all other states, $|s|^2$ attain the same value, 1.5×10^{-34}.

B. EFFECTS OF THE AMPLITUDE OF THE HIGH-FREQUENCY FORCE

Here, the high-frequency field excitation is activated and its amplitude G varied between 0 and 0.5 while keeping its frequency Ω fixed at $\Omega = n\omega$, where $n = 5$ is a positive integer. The range of values of the low-frequency ω was appropriately chosen to ensure the existence of resonances as discussed in Sec. III A. For all values of the positive, negative and zero potential constant considered, we observed a decrease in $|s|^2$ to a minimum value as G increases, and then an increase with further increase in G as well as a monotonic increase in the first-order probability amplitude $|s|^2$ with both the low-frequency and high-frequency driving forces. Henceforth, we refer to the former behavior as *quantum vibrational antiresonance* (QVAR). We note that the results for $c_h = -0.2$ are similar to those for $c_h = 0.2$. Thus, we focus only on two cases: $c_h = 0$ and $c_h = 0.2$. The first-order transition probability exhibits QVAR at certain values of ω as G is varied for fixed $\Omega = n\omega$. For fixed Ω, QVAR was realized for all bound states of the TH quantum well for appropriate choices of ω. In what follows, specific occurrences of QVAR states are discussed for $\omega = 1, 1.7, 2, 3, 4, 5$.

1. $|s|^2$ for Zero Potential constant

We begin our discussion by exploring the QVAR phenomenon with the potential constant set to zero ($c_h = 0$). Note that the system under consideration then reduces to the Morse oscillator given by Eqn (4) [7]. Figure 5(a) shows the transition amplitude, $|s|^2$ for $\omega = 1.0$ and for all the states. For the bound states $f = 1$, 2, 3, and 4 the transition amplitude increases monotonically with G. Here, no QVAR is observed for any of the states. Moreover for the state $f = 0$ the quantity $|s|^2$ is identically zero. In Figure 5(b), for $\omega = 1.7$, QVAR is evidently well pronounced for only one state, $f = 0$ at $g = 0.202$ and with the quantity $|s|^2 = 3.58 \times 10^{-9}$ whereas $|s|^2$ increases monotonically with increasing G for all other states. In Figure 5(c) for $\omega = 2.0$, the transition probability amplitudes within the interval of interest for all the states are identically zero. In Figure 5(d), QVAR takes place in two bound states when $\omega = 3.0$. QVAR is marked for the states $f = 1$ and 2 at $g = [0.146, 0.008]$ with quantity $|s|^2 = [1.37 \times 10^{-32}, 3.24 \times 10^{-34}]$ respectively, whereas $|s|^2$ for the states $f = 3$ and 4 increases monotonically while it takes on zero values in state $f = 0$. Again, for $\omega = 4.0$, $|s|^2$ takes on zero values for all the states as shown in Figure 5(e). However, when the value of ω increases appreciably, QVAR re-appears. For instance, when $\omega = 5.0$, shown in Figure 5(f) marked manifes-
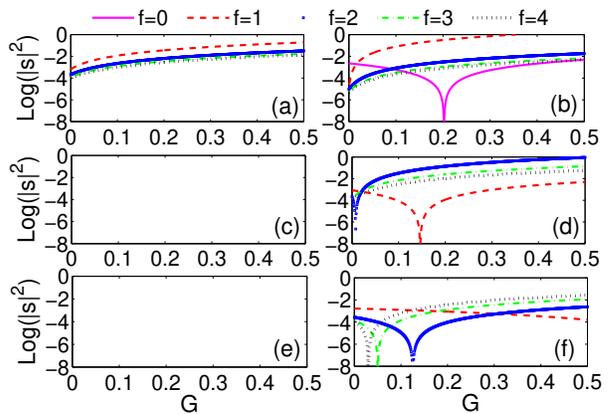

FIG. 5. (Colour online) Quantum vibrational antiresonance (QVAR) in the low-frequency force regime of Tietz-Hua quantum oscillator with zero potential constant, $c_h = 0$. (a) $\omega = 1.0$, (b) $\omega = 1.7$, (c) $\omega = 2.0$, (d) $\omega = 3.0$, (e) $\omega = 4.0$, (f) $\omega = 5.0$
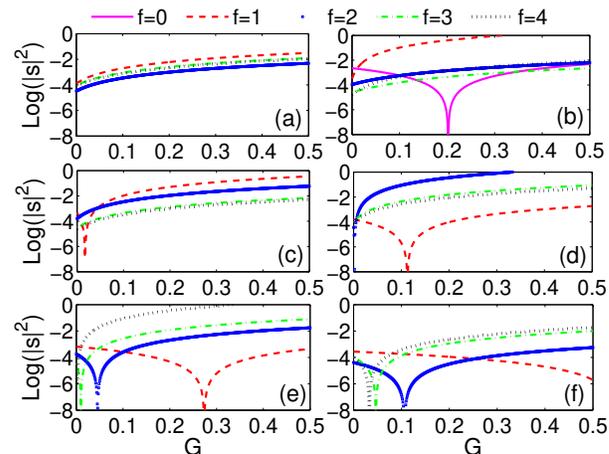

FIG. 6. (Colour online) Quantum vibrational antiresonance (QVAR) in the low-frequency force regime of Tietz-Hua quantum oscillator with positive potential constant, $c_h = 0.2$. (a) $\omega = 1.0$, (b) $\omega = 1.7$, (c) $\omega = 2.0$, (d) $\omega = 3.0$, (e) $\omega = 4.0$, (f) $\omega = 5.0$

tations of QVAR are observed for three states, namely $f = 2, 3$ and 4 at $g = [0.125, 0.05, 0.03]$ with the quantity $|s|^2 = [5.38 \times 10^{-35}, 1.06 \times 10^{-3}, 1.22 \times 10^{34}]$ respectively. The transition probability amplitude within the interval of interest for the state $f = 1$ is nearly constant while that of $f = 0$ varnishes.

2. $|s|^2$ for Positive Potential constant

Now we turn to the case when $c_h \neq 0$ and, in particular, the case when it takes on positive values ($c_h = 0.2$) with. We then find QVAR occurring more frequently

in nearly all the bound states, including bound states where QVAR does not occur when $c_h = 0$ as shown in Figure 5(c,e). For the purpose of comparison with the Morse case (i.e. $c_h = 0$) shown in Figure 5, Figure 6(a) illustrates the transition probability amplitude for $\omega = 1.0$ under the same conditions as in Figure 5(a). For the states $f = 1, 2, 3$, and 4, the transition probability amplitude increases monotonically with G, with no occurrence QVAR in any of the bound states and, similarly to the $c_h = 0$ case, the quantity $|s|^2$ vanishes for the bound state $f = 0$. However, a dramatic change from the zero values obtained for $c_h = 0$, to non-zero values, takes place and the occurrence of $|s|^2$ minima is evident in Figure 6(b) for $\omega = 1.7$. It indicates the QVAR state for $f = 0$ at $G = 0.202$, with the quantity $|s|^2 = 3.58 \times 10^{-9}$ at $|s|^2_{min}$. For the other bound states, $f = 1, 2, 3$, and 4 the transition probability amplitude monotonically increases with varying G. Further increase in ω to $\omega = 2.0$ induces QVAR in the bound state $f = 1$ only at $G = 0.017$ as shown Figure 6(c) while $|s|^2$ is identically zero for $f = 0$, and increases monotonically for all other bound states. We emphasize here that the non-varnishing feature of $|s|^2$ in the bound states $f = 2, 3$ and 4, and the occurrence of QVAR, represent some remarkable and new effects of the potential constant, c_h; and are not found in the Morse oscillator for which $c_h = 0$ shown in Figure 5(c). The effect of G shown in Figure 6(d) for $\omega = 3.0$ is identical to the observed features when $c_h = 0$ where two QVAR occur for the state $f = 1$ and 2 at $G = [0.113, 0.002]$ with quantity $|s|^2 = [8.73 \times 10^{-33}, 1.87 \times 10^{-3}]$ respectively, while the transition probability amplitude for the state $f = 0$ is identically zero and for the state $f = 3$ and 4 $|s|^2$ increases monotonically, without the occurrence of QVAR. In Figure 6(e) for $\omega = 4.0$, the QVAR states are abundant for almost all the bound states, with the exception of the ground state $f = 0$, where the first-order transition probability amplitude within the interval of interest is identically zero. For the state $f = 1, 2, 3$ and 4 the QVAR phenomenon occurs at $G = [0.274, 0.046, 0.01, 0.002]$ with quantity $|s|^2 = [6.3 \times 10^{-33}, 5.53 \times 10^{-34}, 2.16 \times 10^{-34}, 1.62 \times 10^{-34}]$ respectively. Again, the resonance feature at $\omega = 4.0$ is absent for $c_h = 0$ (See Figure 5(e)). In Figure 6(d) three QVAR states are shown for $\omega = 5.0$ of the five states, namely, $f = 2, 3$ and 4 and occur at $G = [0.106, 0.046, 0.033]$ with $|s|^2 = [6.53 \times 10^{-35}, 1.09 \times 10^{-34}, 1.2 \times 10^{-34}]$ respectively. However, there is gradual decrease in the first-order transition probability amplitude for the bound state $f = 1$ while that of $f = 0$ is identically zero.

At this juncture, we make two remarks: (i) the main effect of the high-frequency signal on the Tietz-Hua oscillator is the induction of new QVAR states when $c_h \neq 0$; and (ii) QVAR occurs in a single quantum oscillator in the absence of coupling, unlike classical vibrational antiresonance (VAR) which can only take place in coupled nonlinear oscillators [49].
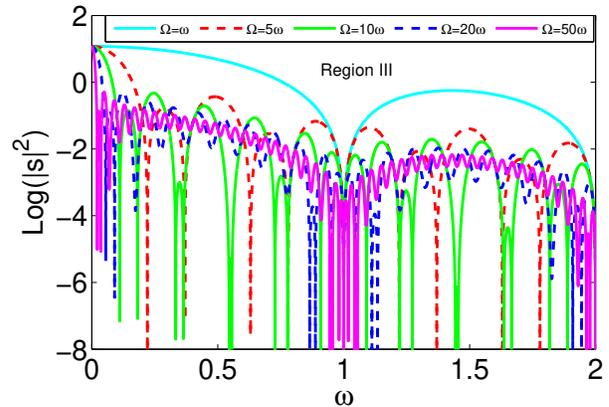

FIG. 7. (Colour online) Effects of high-frequency on $|s|^2$ in the ground state $f = 0$, for different values of $\Omega = n\omega$ scaled as $n = 1, 5, 10, 20$ and 50. The other parameters are: $c_h = 0.2$, $F = 0.05$ and $G = 0.5$
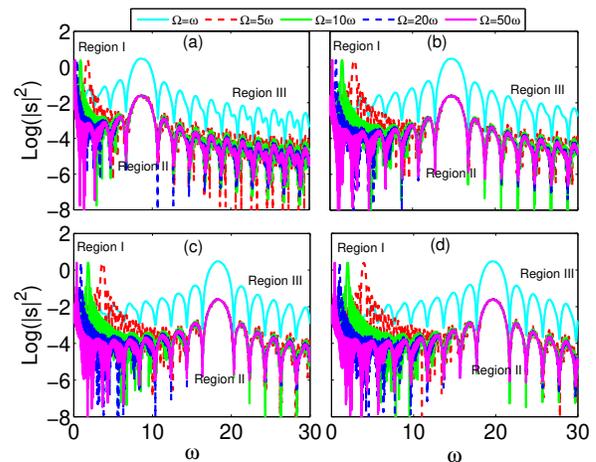

FIG. 8. (Colour online) Effects of high-frequency on $|s|^2$ in the excited states $f = 1, 2, 3$ and 4 for different values of $\Omega = n\omega$ scaled as $n = 1, 5, 10, 20$ and 50. The other parameters are: $c_h = 0.2$, $F = 0.05$ and $G = 0.5$.

C. EFFECT OF HIGH-FREQUENCY ON THE TRANSITION PROBABILITY

In the presence of the second harmonic force we investigate the impact of its high-frequency component Ω on the first-order transition probability for the states, and henceforth we focus on the positive potential constant ($c_h = 0.2$). In Eq. (19) the high-frequency component Ω appears in the arguments of r_{2+} and r_{2-} which are sinusoidal functions of the first-order transition probability. Thus, the first-order transition probabilities can exhibit sequences of resonance peaks when Ω is varied while the other parameters of the external field remain fixed. The high-frequency Ω, is set as an integer multi-

ple of the low-frequency (i.e. $\Omega = n\omega$) with n denoting the integer scaling factor so that Ω varies with the low-frequency ω. The effect of Ω on $|s|^2$ with $n = 1, 5, 10, 20$, and 50, was first investigated for all the bound states and $c_h = 0.2$ of the TH quantum wells within three regions of interest i.e.: Region I: $\omega < \omega_{fi}$, Region II: $\omega \approx \omega_{fi}$ and Region III: $\omega > \omega_{fi}$. In addition, we chose appropriate values for n and examined extensively the behavior of the transition probability as a function of ω under the combined effects of the two harmonic fields. For all the cases considered here, the effect of the high-frequency component is observed numerically from the variation of the quantity $\ln |s|^2$ with the low-frequency (ω); the amplitudes of the two forces each remain fixed at F=0.05 and $G = 0.5$.

We now examine the effect of the high-frequency component on different states (i.e. for $f \in [0:4]$) starting with the ground state, $f = 0$. Remarkably, it is impracticable to examine the effect of $\Omega = n\omega$ on the transition probability for the state $f = 0$ in the Regions I ($\omega < \omega_{fi}$) and II ($\omega \approx \omega_{fi}$) since $\omega_{fi} = 0$ for all values of the potential constant. However, it is clear from Figure 7 that the transition probability for the ground state for $c_h = 0.2$ in Region III is rapidly oscillating from its maximum value at $\omega \approx \omega_{fi} = 0$ with multiple peaks occurring sequentially for $n \in [5, 10, 20, 50]$, with the number of peaks increasing appreciably with increase in the values of n over the entire region. This scenario was also found for all values of c_h. However, when the systems does not vibrate, i.e. for $n = 1$, the transition probability is characterized by slowly varying peaks with its minimum occurring at integer values of ω over the given interval.

Next, we examine extensively the excited states of the oscillator. Illustrated in Figure 8 and in the 3-D plot displayed in Figures 9 are sample results for the different states (i.e. for $f \in [1:4]$). The behavior of the transition probability in each of the Regions I, II and III was examined thoroughly and is summarized below.

1. Region I: $\omega < \omega_{fi}$

The scaling integer n plays a significant role in the vibrational dynamics. Clustered peaks dominate this low-frequency regime of ω with the order of the onset of peaks occurring with decreasing magnitudes of the integer n (see Figure 8). Prominent multiple peaks with marked intensities occur in the reversed order: $n = 50, 20, 10$ and 5. However, for $n = 1$ (i.e. $\Omega = \omega$), when the system does not vibrate, the states show a sequence of slowly varying peaks with increasing intensity. This reversal in the peak intensity can be understood as follows. The r_{2-} component of the probability amplitude s, given by Eq. (19) (See Appendix) increases appreciably with increasing n, thus attaining its maximum rapidly at low ω values. The transition probability does not exhibit a monotonic behavior within this region in all the states; rather, it oscillates rapidly with increasing n. The maximum peak points for $\Omega = n\omega$, with $n = 5, 10, 20$ and 50 for the states $f = 1, 2, 3$ and 4 are attained when the high-frequency component of the bi-harmonic force equals the transition frequency of the given state (i.e. $\Omega = n\omega = \omega_{fi}$). The characteristics features of the transition probability in this region are analogous to the vibrational higher-order resonance observed in the classical system [13].

2. Region II: $\omega \approx \omega_{fi}$

In this region, for states $f = 1, 2, 3$ and 4 with $c_h = 0.2$, the dominant peak is obtained when $\Omega = \omega$ (i.e. $n = 1$). This is to be expected judging from Eq. (19) where it can be inferred directly that the r_{1-} and r_{2-} components are equal, with their respective denominator at its minimum value, with $|s|^2$ attaining its maximum value when $\Omega = \omega = \omega_{fi}$. The QVR in this case is analogous to the traditional resonance observed with the low-frequency force acting alone, but differs from it in that the second harmonic force also has its frequency equal to that of transition frequency of the given state. This consequently gives rise to the increase in transition probability with the amplitude G and frequency component Ω of the second harmonic force. The minimization of the denominator of the r_{1-} component of the transition amplitude increases the transition probability appreciably in this region for $n = 5, 10, 20$ and 50 corresponding to the pronounced QVR peaks exhibited by the transition frequencies of the oscillator as shown in (See Figure 8).

3. Region III: $\omega > \omega_{fi}$

In this region for all the states ($f = 1, 2, 3$ and 4) with $c_h = 0.2$ fixed, the transition probability exhibits multiple peaks of varying amplitude for $n = 5, 10, 20$ and 50. For $n = 1$, however, $|s|^2$ oscillates slowly with sequential peaks of decreasing amplitude, without any prominent maximum peak, as ω increases.

IV. QVR REGIME IN PARAMETER-SPACE: TRANSITION FROM QVAR TO QVR

In this section, we describe the results of numerical experiments using several different values of the scaling integer n. Shown in Figure 9(a,b) is the dependence of $|s|^2$ on the parameters ω and G for $n = 1$. Notice that Figure 9 is a 3-D representative of Figure 5 in which the occurrence of QVAR was demonstrated in section IV(B) for selected values of the low-frequency, ω. The 3-D representation provides further insight into the parameter space of ω and G in which resonance is expected to occur. With $\Omega = n\omega$ and $n = 1$, we find in Figure 9 that all the excited bound states exhibit QVAR. However, the location and number of QVAR dips/wells is dependent on

the bound state, $f = i(i = 1, \ldots, 4)$. Starting with the state $f = 1$, and in the low amplitude regime of the high-frequency component of the driving force, three distinct and separated QVAR dips are clearly visible, all of which occur within the interval $0 < G < 0.3$. Moving further from $f = 1$ to higher excited bound states $f = 2, 3, 4$, the QVAR states become closely bunched in the neighbourhood of $G < 0.05$ with vanishing QVAR. This observed QVAR resonance feature predominates when $n < 50$. The existence of the dips in parameter space shown in Figure 9(a,b) suggests the likelihood of particle trapping in energy states low compared to the higher excited energy states. However, when the intensity of the high-frequency component of the driving becomes stronger, the trapping probability tends to zero during the transition.

When the scaling integer, n becomes large such that $\Omega \gg \omega$, there is a dramatic reversal in the nature of the resonance oscillation in which a transition from QVAR to QVR occur. Here, QVR occurs when $n = 50$ as shown in Figure 9(c,d). Two of the most striking features evident in Figure 9(c,d) are the increase in peak densities and the appearance of new peaks in the excited bound state, i.e. $f_i(i = 1, \ldots, 4)$ of the Tietz-Hua oscillator. The observed features are characteristic of QVR induced by the high-frequency component, Ω of the second harmonic field. The phenomenon appears more pronounced in the low ω regime (typically, $\omega = [0, 1]$) for all states in which $|s|^2$ exhibits multiple resonances as well as sharply defined maximum transition probability as shown in Figure 10.

In the preceding discussions, we had set the potential parameter $c_h = 0$ corresponding to the Morse potential and chosen an arbitrary value ($c_h = 0.2$) for the TH potential system. In diatomic molecules, c_h can take on a wide range of both negative and positive values (See for instance Ref. [41, 42, 50, 51]) which determines the rotation-vibration spectrum of a given molecular system explicitly. We now consider the behaviour of $|s|^2$ over wide ranges range of the parameters c_h and G, and its impact on resonance. Illustrated in Figure 10 is the variation of $|s|^2$ as functions of c_h and G. Simulations were carried out for all the bound states and for different values of the low-frequency $\omega[1.0, 1.7, 3.0, 5.0]$ while fixing other system parameters. For the state $f = 1$, QVAR is predominant for all values of c_h with the QVAR depth located in the neighbourhood of $G = 0.1$ when $\omega = 3.0$. In the state $f = 2$, however, QVAR occurs abundantly at higher values of ω, namely, $\omega = 5.0$ and as higher energy states are approached ($f = 4$) the QVAR seems to disappear, with QVR features (indicated by the red-coloured regions) predominating.

V. SUMMARY AND CONCLUSIONS

In summary, the phenomenon of vibrational resonance (VR) occurs when the response of a low-frequency driven classical oscillator is enhanced by means of a second, but high-frequency signal whose frequency is comparatively very strong relative to the low-frequency force. In this paper, we have investigated the quantum counterpart of this phenomenon in a quantum mechanical Tietz-Hua oscillator driven by a dual-frequency field, consisting of weak and strong contributions at different frequencies. We explored, identified and classified the varieties of resonances induced by the high-frequency vibration characterized by the appearance of minima and maxima of the first-order transition probability amplitude, $|s|^2$. With only the low-frequency ω component of the driving force, $|s|^2$ exhibited a sequence of resonances of decreasing amplitude, with the dominant resonance occurring at the low-frequency ω equal to the transition frequency of the bound state under consideration. However, under the combined actions of the low-frequency and the high-frequency excitations, we found some interesting resonance phenomena, which we clasify as follows: *quantum vibrational resonance* (QVR) wherein a maximum or peak in $|s|^2$ occur, *quantum vibrational antiresonance* (QVAR) wherein a minimum or dip in $|s|^2$ occur and *quantum vibrational multiresonance* (QVMR) wherein either or both QVR and QVAR occur in two or more bound states, or in a given parameter space.

Conclusively, it was found that the high-frequency excitation field significantly enhances the transition probability of the bound states when its frequency is very large in comparison with ω - typically, $\Omega = 50\omega$ in the low-frequency ω regime where it may be considered otherwise weak in the presence of a single harmonic force. Notably, the amplitude G of the high-frequency external field induces QVAR modes in all of the states considered, depending on the values of ω. In addition, by setting the high-frequency component Ω to be an integer multiple of the low-frequency ω component, QVMR appeared, in addition to pronounced maximum intensities, and were found to characterize the excited energy states. The onset of maxima depended on the magnitude of n when the $\omega < \omega_{fi}$, ω_{fi} being the transition frequencies. Finally, in the two-parameter space of $\omega - G$, a transition from QVAR to QVR, wherein peaks in $|s|^2$ predominates was found when $n \approx 50$. For $n < 50$ in the $\omega - G$ parameter space, QVAR predominates in all the bound states.

APPENDIX: QUANTUM THEORY OF VIBRATIONAL RESONANCE

In principle, a quantum mechanical oscillator undergoes transitions between the energy eigenstates when subjected to an external field. It is therefore justifiable to focus our attention on determining the probability of finding the oscillator in any f_{th} state at time t (See Ref. [7] for details). The starting point is to consider the time-dependent Schrödinger equation for any quantum mechanical system given as
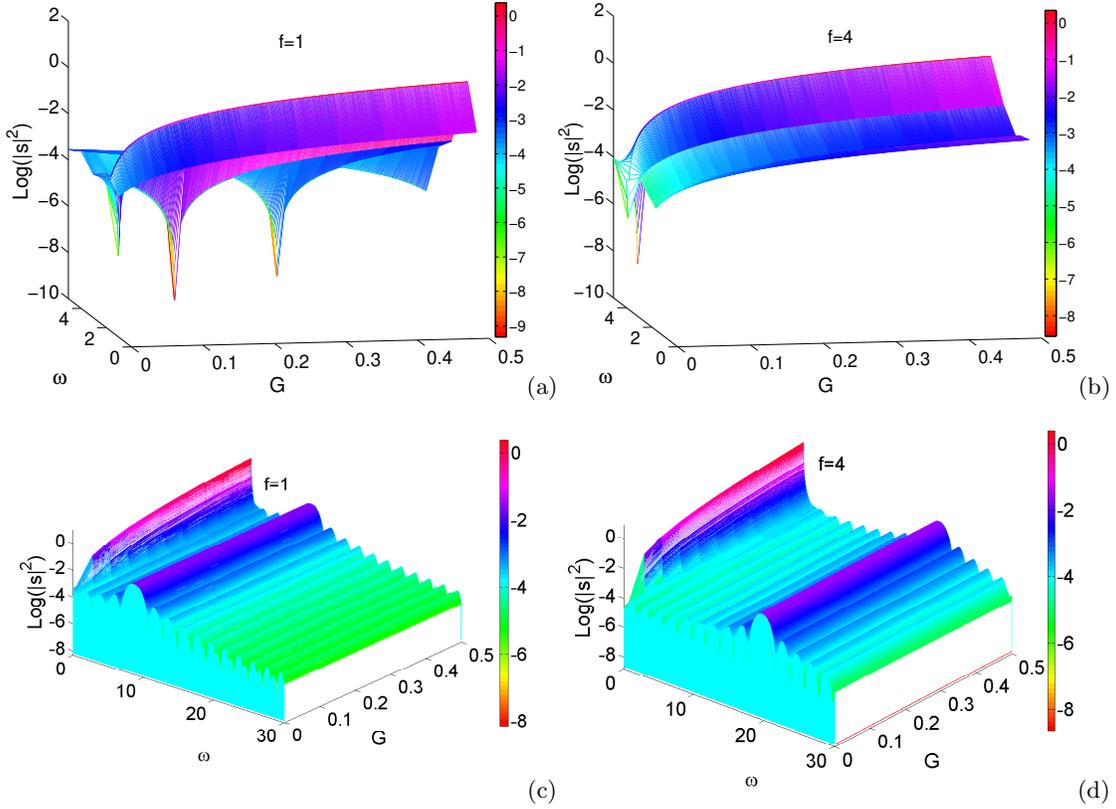
$$ih\frac{\partial \psi}{\partial t} = H\psi, \tag{6}$$

FIG. 9. (Colour online) Three-dimensional views of the transition probability $|s|^2$ as function of ω and G showing the effects of high-frequency for integer multiples of $\Omega(\Omega = n\omega)$: (a),(b) $n = 1$; and (c),(d) $n = 50$; $c_h = 0.2$ and $g = 0.05$.

where $\psi(x,t)$ is the wave function of the perturbed system, which may be written as

$$\psi(x,t) = \sum_n a_n(t)\phi_n(x)e^{-\frac{iE_n}{\hbar}t}. \qquad (7)$$

The probability of finding the system in the state n is

$$P_n(t) = |a_n(t)|^2; \quad \text{with} \quad \sum_n |a_n(t)|^2 = 1. \qquad (8)$$

To determine the probability amplitude, $a_n(t)$, we apply standard time-dependent perturbation theory. Suppose the external field is switched-on at $t = 0$ and switched-off at $t = T$, i.e. after a finite time interval T. Suppose also that the system was initially in the ith state with the eigenfunction ϕ_i. Then, at $t = 0$ the probability of finding the system in the ith state is 1 and the probability of finding the system in any other state is 0, that is, $a_n(0) = \delta_{ni}$. Under the influence of the applied fields, the system can make a transition from the ith state to another state after time T. Once the perturbation is switched-off, the system settles into a stationary state and this final state is denoted as f.

Substituting Eq. (7) into Eq. (6) yields

$$i\hbar \sum_n \dot{a}_n e^{-\frac{iE_n}{\hbar}t}\phi_n = \lambda \sum H_1^0 e^{-\frac{iE_n}{\hbar}t}, \qquad (9)$$

where $H_1^0 = W(x)e^{-i\omega t}$. Multiplying Eq. (9) by ϕ_f^* and integrating over all space, we have

$$i\hbar \dot{a}_f = \lambda a_n e^{-i(\omega_{f_n} - \omega)t} H_{f_n} \qquad (10)$$

where

$$\omega_{f_n} = (E_f - E_i)/\hbar \quad \text{and} \qquad (11)$$

$$H_{f_n} = \oint_{-\infty}^{\infty} \phi_f^* W(x)\phi_n dx. \qquad (12)$$

Expanding $a_f(t) = a_f^{(0)} + \lambda a_f^{(1)} + \lambda^{(2)} a_f^{(2)} + \ldots$, we obtain the evolutions for a_f^0 and a_f^1 as

$$i\hbar \dot{a}_f^{(0)} = 0 \qquad (13)$$

$$i\hbar \dot{a}_f^{(1)} = \sum a_n^0 e^{i(\omega_{f_n} - \omega)t} H_{f_n} \qquad (14)$$

Thus, Eq. (13) gives $a_f^{(0)} = a_f^t$.

Eq. (14) is a set of coupled integro-differential equations. For a system with n discrete eigenstates Eq. (14) consists of n equations, each of which has n terms on the right-side. To simplify the problem, we modify it slightly by assuming that the perturbation is switched-on at $t = 0$ and switched-off at $t = T$. At $t = 0$ the system may be assumed to reside in the eigenstate ϕ_i such
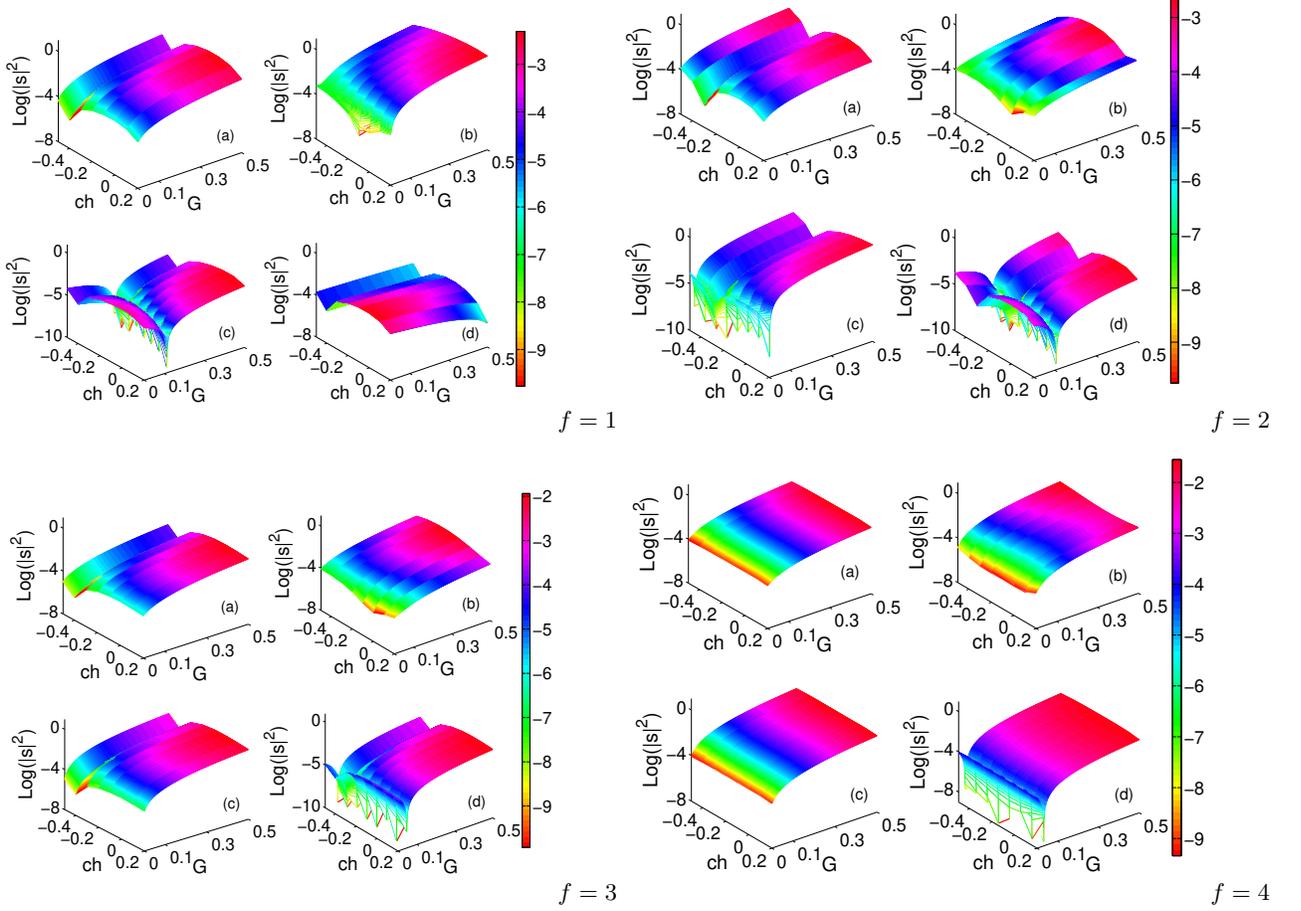
FIG. 10. (Colour online) Three-dimensional view of the transition probability $|s|^2$ as functions of both c_h and G showing the effects of high-frequency for integer multiples of $\Omega(\Omega = n\omega)$, where $n = 5$ is an integer and $g = 0.05$. Subplots labelled (a-d) correspond to different values of the low-frequency ω fixed as $[1, 1.7, 3, 5]$. (a) $f = 1$, (b) $f = 2$, (c) $f = 3$ and (d) $f = 4$.

that $a_{ni}^0 = \delta_{ni}$. Once the perturbation is switched-off the system settles down to a stationary final state denoted by f. We are interested in the probability of finding the system in the state f after time T. This probability is denoted as $P_{f_i} = a_f^* a_f$. Eq. (14) may be written as

$$\dot{a}_f^{(1)} = \frac{1}{i\hbar} e^{-i(\omega_{f_{f_i}} - \omega)t} H_{f_i}. \quad (15)$$

Integrating Eq. (15) from 0 to T gives

$$a_f^{(1)}(T) = \frac{H_{f_1}}{i\hbar} \int_0^T e^{-i(\omega_{f_{f_i}} - \omega)t} dt,$$
$$= \frac{H_{f_1}}{\hbar(\omega_{f_i} - \omega)} \left(1 - e^{-i(\omega_{f_{f_i}} - \omega)T}\right). \quad (16)$$

Then,

$$P_{f_i}(T) = \frac{4|H_{f_i}|^2}{\hbar^2(\omega_{f_i} - \omega)^2} \sin^2\left[(\omega_{f_i} - \omega)\right] T/2. \quad (17)$$

For $H_1 = x(g\cos(\omega t) + G\cos(\Omega t))$,

$$a_f(T) = \frac{H_{f_1}}{2\hbar} s, \text{ with } s = g(r_{1+} + r_{1-}) + G(r_{2+} + r_{2-}), \quad (18)$$

and $r_{1\pm}$ and $r_{2\pm}$ given, respectively as

$$r_{1\pm} = \frac{1 - e^{i(\omega_{f_1} \pm \omega)T}}{(\omega_{f_1} \pm \omega)}, \quad r_{2\pm} = \frac{1 - e^{i(\omega_{f_1} \pm \Omega)T}}{(\omega_{f_1} \pm \Omega)} \quad (19)$$

$$H_{f_i} = \oint_{-\infty}^{\infty} \phi_f^* x \phi_i dx. \quad (20)$$

The transition probability from the ith state to the fth state is therefore given by $P_{f_i}(T)|\delta_{f_i} + \lambda a_f^{(1)}(T)|^2$, where s depends solely on the parameters of the bi-harmonic forcing and T.

[1] Vadim S. Anishchenko, Tatyana E. Vadivasova, and Galina I. Strelkova, *Deterministic Nonlinear Systems*, 1st ed. (Springer-Verlag Berlin Heidelberg, Germany, 2014).

[2] M. Gitterman, *The Noisy Oscillator: Random Mass, Frequency, Damping*, 2nd ed. (World Scientific, Singapore, 2013).

[3] Anton Quelle and Cristiane Morais Smith, "Resonances in a periodically driven bosonic system," Phys. Rev. E, **96**, 052105 (2017).

[4] Sansan Li, Xingang Wang, and Shuguang Guan, "Periodic coupling suppresses synchronization in coupled phase oscillators," New J. Phys., **20**, 113013 (2018).

[5] L. Schimansky-Geier, V.S. Anishchenko, and A. Neiman, "Chapter 2 phase synchronization: From periodic to chaotic and noisy," in *Neuro-Informatics and Neural Modelling*, Handbook of Biological Physics, Vol. 4, edited by F. Moss and S. Gielen (North-Holland, 2001) pp. 23–82.

[6] Emanuel F. de Lima and R. Egydio de Carvalho, "Effects of oscillatory behavior of the dipole function on the dissociation dynamics of the classical driven Morse oscillator," Physica D: Nonlinear Phenomena, **241**, 1753–1757 (2012).

[7] S. Rajasekar and M. A. F. Sanjuán, *Nonlinear Resonances, Springer Series in Synergetics* (Springer, Switzerland, 2016).

[8] M. Plodzień and M. M. Wysokiński, "Rabi-resonant behavior of periodically driven correlated fermion systems," Phys. Rev. B, **100**, 041116 (2019).

[9] P. S. Landa and P. V. E. McClintock, "Vibrational resonance," J. Phys. A: Math. Gen., **33**, L433 (2000).

[10] M. Gitterman, "Bistable oscillator driven by two periodic fields," J. of Phys. A: Math. & Gen., **34**, L355 (2001).

[11] Iliya I Blekhman, *Vibrational Mechanics* (World Scientific, Singapore, 2000).

[12] I. I. Blekhman and P. S. Landa, "Conjugate resonances and bifurcations in nonlinear systems under biharmonical excitation," Intern. J. Non-Lin. Mech., **39**, 421 – 426 (2004).

[13] V. N. Chizhevsky, "Vibrational higher-order resonances in an overdamped bistable system with biharmonic excitation," Phys. Rev. E, **90**, 042924 (2014).

[14] V. N. Chizhevsky, E. Smeu, and G. Giacomelli, "Experimental evidence of vibrational resonance in an optical system," Phys. Rev. Lett., **91**, 220602 (2003).

[15] V. N. Chizhevsky, "Experimental evidence of vibrational resonance in a multistable system," Phys. Rev. E, **89**, 062914 (2014).

[16] V. N. Chizhevsky, "Noise-induced suppression of nonlinear distortions in a bistable system with biharmonic excitation in vibrational resonance," Phys. Rev. E, **92**, 032902 (2015).

[17] J. P. Baltanás, L. López, I. I. Blechman, P. S. Landa, A. Zaikin, J. Kurths, and M. A. F. Sanjuán, "Experimental evidence, numerics, and theory of vibrational resonance in bistable systems," Phys. Rev. E, **67**, 066119 (2003).

[18] K. Abirami, S. Rajasekar, and M. A. F. Sanjuán, "Vibrational resonance in the Morse oscillator," Pramana, **81**, 127–141 (2013).

[19] S. Rajasekar, K. Abirami, and M. A. F. Sanjuán, "Novel vibrational resonance in multistable systems," Chaos, **21**, 033106 (2011).

[20] J. H. Yang and X. B. Liu, "Controlling vibrational resonance in a multistable system by time delay," Chaos, **20**, 033124 (2010).

[21] Tianqi Qin, Tianting Xie, Maokang Luo, and Ke Deng, "Vibrational resonance in fractional-order overdamped multistable systems," Chin. J. of Phys., **55**, 546 – 555 (2017).

[22] Muhammet Uzuntarla, Ergin Yilmaz, Alexandre Wagemakers, and Mahmut Ozer, "Vibrational resonance in a heterogeneous scale free network of neurons," Commun. Nonl. Sci. Numer. Simulat., **22**, 367–374 (2015).

[23] Canjun Wang, KeLi Yang, and Shi-Xian Qu, "Vibrational resonance in a discrete neuronal model with time delay," Intern. J. Mod. Phys. B, **28** (2014).

[24] Yingmei Qin, Chunxiao Han, Yanqiu Che, and Jia Zhao, "Vibrational resonance in a randomly connected neural network," Cognitive Neurodynamics (2018) 12:509518, **12**, 509–518 (2018).

[25] K. Abirami, S. Rajasekar, and M. A. F. Sanjuán, "Vibrational resonance in a harmonically trapped potential system," Commun. Nonlin. Sci. and Numer. Simulat., **47**, 370 – 378 (2017).

[26] T. O. Roy-Layinde, J. A. Laoye, O. O. Popoola, and U. E. Vincent, "Analysis of vibrational resonance in biharmonically driven plasma," Chaos, **26**, 093117 (2016).

[27] T. O. Roy-Layinde, J. A. Laoye, O. O. Popoola, U. E. Vincent, and P. V. E. McClintock, "Vibrational resonance in an inhomogeneous medium with periodic dissipation," Phys. Rev. E, **96**, 032209 (2017).

[28] U. E. Vincent, T. O. Roy-Layinde, O. O. Popoola, P. O. Adesina, and P. V. E. McClintock, "Vibrational resonance in an oscillator with an asymmetrical deformable potential," Phys. Rev. E, **98**, 062203 (2018).

[29] M. I. Dykman, D. G. Luchinsky, R. Mannella, P. V. E. McClintock, N. D. Stein, and N. G. Stocks, "Stochastic resonance in perspective," Il Nuovo Cimento D, **17**, 661–683 (1995).

[30] J. Casado-Pascual, J. Gómez-Ordónez, and M. Morillo, "Stochastic resonance: theory and numerics." Chaos, **15**, 26115 (2005).

[31] D. Witthaut, "Stochastic resonance driven by quantum shot noise in superradiant Raman scattering," J. Phys. B: At. Mol. Opt. Phys., **45**, 225501 (2012).

[32] S. F. Huelga and M. B. Plenio, "Quantum stochastic resonance in electron shelving," Phys. Rev. A, **62**, 052111

(2000).

[33] B. Fan and M. Xie, "Stochastic resonance in a tristable optomechanical system," Phys. Rev. A, **95**, 023808 (2017).

[34] Susana F. Huelga and Martin B. Plenio, "Stochastic resonance phenomena in quantum many-body systems," Phys. Rev. Lett., **98**, 170601 (2007).

[35] Milena Grifoni and Peter Hänggi, "Coherent and incoherent quantum stochastic resonance," Phys. Rev. Lett., **76**, 1611–1614 (1996).

[36] H. H. Adamyan, S. B. Manvelyan, and G. Yu. Kryuchkyan, "Stochastic resonance in quantum trajectories for an anharmonic oscillator," Phys. Rev. A, **63**, 022102 (2001).

[37] J. A. Kunc and F. J. Gordillo-Vázquez, "Rotational–vibrational levels of diatomic molecules represented by the Tietz–Hua rotating oscillator," J. Phys. Chem. A, **101**, 1595–1602 (1997).

[38] P. M. Morse, "Diatomic molecules according to the wave mechanics. II. Vibrational levels," Phys. Rev., **34**, 57–64 (1929).

[39] W. Hua, "Four-parameter exactly solvable potential for diatomic molecules," Phys. Rev. A, **42**, 2524–2529 (1990).

[40] F. J. Gordillo-Vázquez and J. A. Kunc, "Radial probability distributions of atoms in diatomic molecules represented by the rotating Morse and Tietz-Hua oscillators," J. Mol. Struct.: THEOCHEM, **425**, 263 – 270 (1998).

[41] M. Hamzavi, A. A. Rajabi, and H. Hassanabadi, "The rotationvibration spectrum of diatomic molecules with the TietzHua rotating oscillator and approximation scheme to the centrifugal term," Molecular Phys., **110**, 389–393 (2012).

[42] M. Hamzavi, A. A. Rajabi, and K. E. Thylwe, "The rotation-vibration spectrum of diatomic molecules with the Tietz-Hua rotating oscillator," Inter. J. Quan. Chem., **112**, 2701–2705 (2012).

[43] Amlan K. Roy, "Ro-vibrational spectroscopy of molecules represented by a TietzHua oscillator potential," J. Math. Chem., **52**, 14051413 (2014).

[44] R. Khordad and B. Mirhosseini, "Application of Tietz potential to study singlet-triplet transition of a two-electron quantum dot," Comm. Theor. Phys., **62**, 77–80 (2014).

[45] E. B. Al, E. Kasapoglu, S. Sakiroglu, C. A. Duque, and I. Sökmen, "Binding energy of donor impurity states and optical absorption in the Tietz-Hua quantum well under an applied electric field," J. Mol. Struct.: THEOCHEM, **1157**, 288–291 (2018).

[46] H. Sari, E. Kasapoglu, S. Sakiroglu, and I. Skmen, "Position-dependent mass effects on the optical responses of the quantum well with TietzHua potential," Optik, **178**, 1280–1284 (2019).

[47] E. Kasapoglu, S. Sakiroglu, F. Ungan, U. Yesilgul, C. A. Duque, and I. Sökmen, "Optical properties of the Tietz-Hua quantum well under the applied external fields," Physica B, **526**, 127–131 (2017).

[48] F. Ungan, H. Sari, E. Kasapoglu, U. Yesilgul, S. Sakiroglu, and I. Sökmen, "Study of electron-related optical responses in the Tietz-Hua quantum well: Role of applied external fields," Photonics and Nanostructures - Fundamentals and Applications, **32**, 47–52 (2018).

[49] P. Sarkar and D. S. Ray, "Vibrational antiresonance in nonlinear coupled systems," Phys. Rev. E, **99**, 052221 (2019).

[50] A. Khodja, F. Benamira, and L. Guechi, "Comment on the rotationvibration spectrum of diatomic molecules with the Tietz-Hua rotating oscillator," Intern. J. Quantum Chem., **117**, e25334 (2017).

[51] A. Khodja, A. Kadja, F. Benamira, and L. Guechi, "Complete non-relativistic bound state solutions of the Tietz-Wei potential via the path integral approach," Eur. Phys. J. Plus, **134**, 57 (2019).